Uncertainty of ESD Pulse Metrics Due to Dynamic Properties of Oscilloscope

Janusz Baran and Jan Sroka, *Senior Member, IEEE*

***Abstract*—This paper investigates how dynamics of an HF oscilloscope affects standardized metrics (i.e., rise time and peak value) of a recorded electrostatic discharge (ESD) current pulse and evaluates the oscilloscope measurement uncertainty. A frequency-domain dynamic model of the oscilloscope, based on measurements of the input reflection and voltage gain magnitude, is derived. The complex voltage gain is approximated with a transfer function to take into account unmeasured phase shift. A high-order discrete-time filter is designed to fit the measured voltage gain magnitude not only in the passband, but also beyond it as well. Since the measured data are burdened with measurement uncertainties, the worst-case deviations of the oscilloscope input impedance and the voltage gain (in the form of envelopes of the frequency responses) are calculated, and components of Type B uncertainty of the ESD pulse metrics corresponding to these deviations are estimated using the sensitivity method.**

***Index Terms*—Frequency-domain analysis, modeling, oscilloscopes, transfer functions, uncertainty.**

I. INTRODUCTION

A MEASUREMENT chain for calibration of an electrostatic discharge (ESD) pulse consists of a target (current–voltage transducer), coaxial cables, an attenuator, and an oscilloscope (see Fig. 1).

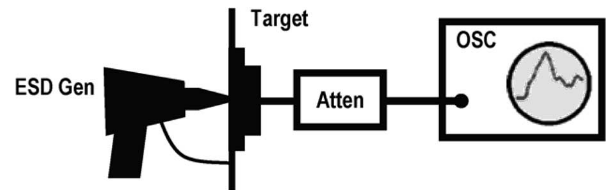

Fig. 1. Setup for pulse measurement in calibration of ESD simulators.

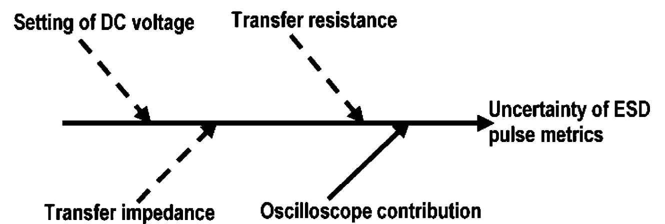

Fig. 2. Fishbone diagram of uncertainty contributions in ESD pulse measurement.

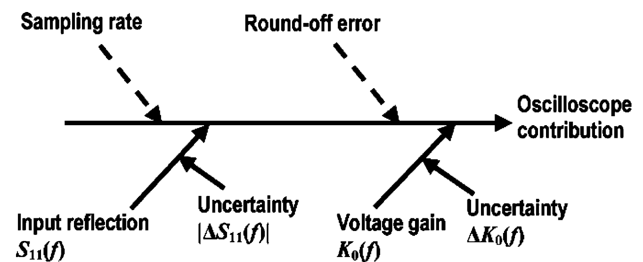

Fig. 3. Oscilloscope uncertainty contributions in ESD pulse measurement.

In this paper, we follow the approach of [3], where the transfer resistance, which is the quotient of the undistorted oscilloscope voltage and the current at the simulator's tip, is used for recalculation of the discharge current. This hypothetical current deviates from the current recalculated with a frequency-dependent model of the measurement chain and the oscilloscope. Estimation of this deviation is meant in this paper as a measurement uncertainty in calibration of the ESD pulse.

Components of uncertainty budget in the ESD pulse calibration are shown in Fig. 2. This paper deals only with the oscilloscope contribution (continuous arrow in Fig. 2). Detailed uncertainty components of the oscilloscope are shown in Fig. 3.

Calibration laboratories are compelled to establish individual uncertainty budget for each measurement, so the battle for reduction of the uncertainty is of prior importance. A simulator under calibration complies with standards only if all its metrics are within the limits even when extended by the uncertainties. In a standard in act [1], the specification limits are $\pm 10\%$ of the standardized nominal pulse peak value and the rise time between 0.7 and 1 ns. Since the best measurement capability of a laboratory is about $\pm 6\%$ for the peak value and ± 0.1 ns for the rise time, the range of measured values to pass the calibration is rather narrow, taking into consideration spread of simulator parameters in manufacturing and their time drift. In the calibration of ESD simulators, an oscilloscope is a component whose analysis has a large potential of diminishing the uncertainty budget.

There are not many papers in which an oscilloscope is taken into account for establishing the uncertainty budget of the ESD pulse measurement. Oscilloscope parameters published in technical specification and relevant in uncertainty estimation, i.e., vertical linearity, vertical accuracy, storage truncation (up to 8 bits), offset accuracy, and time base accuracy, are related to low-frequency behavior. A comprehensive analysis of uncertainty of the whole ESD measurement path (i.e., ESD simulator, current transducer, attenuator, coaxial cable, and oscilloscope) was conducted in [4]. As far as the oscilloscope is concerned,

Manuscript received November 16, 2006; revised June 20, 2007 and January 25, 2008. Current version published November 20, 2008.

J. Baran is with the Institute of Electronics and Control Systems, Czestochowa Technical University, 42–200 Czestochowa, Poland (e-mail: baranj@el.pcz.czest.pl).

J. Sroka is with the EMC-Testcenter Zurich AG, 8052 Zurich, Switzerland (e-mail: j.sroka@emc-testcenter.com).

Digital Object Identifier 10.1109/TEMC.2008.2004597

0018-9375/$25.00 © 2008 IEEE

Authorized licensed use limited to: IEEE Xplore. Downloaded on November 28, 2008 at 09:03 from IEEE Xplore. Restrictions apply.

the authors consider two components of the pulse amplitude uncertainty. The main contribution is the voltage reading. Moreover, the mismatch at the oscilloscope input port, which is a frequency-dependent factor, is also taken into account. The resulting contribution of the oscilloscope in expanded uncertainty of the pulse peak is about 5% for 4 to 6 kV static voltage. The dominant contribution to the rise time uncertainty comes from the sampling rate, but the value of 24 ps, reported in [4] for oscilloscope with 5 GS/s sampling rate seems to be underestimated more than five times.

The oscilloscope rise time $t_{\rm OSC}$, usually published in technical specifications, is practically the only parameter that represents the oscilloscope dynamics. True rise time $t_{\rm TRUE}$ can be recalculated from observed rise time $t_{\rm OBS}$ as $t_{\rm TRUE} = \sqrt{t_{\rm OBS}^2 - t_{\rm OSC}^2}$. However, this formula is exact only for the step Gaussian input signal and an oscilloscope with Gaussian impulse response [5]. It is justified if the measured pulse is within the oscilloscope bandwidth.

Uncertainty budget based on parameters from technical specification of an oscilloscope is questionable because its high-frequency behavior is neglected. This question is particularly justified in measurement of the ESD pulse for which the frequency range (up to 4 GHz [3]) is comparable with the bandwidth of single-shot oscilloscopes currently in use (i.e., 1 GHz according to the International Electrotechnical Commission (IEC) standard in act [1] and at least 2 GHz in the IEC standard to be introduced [3]). More detailed uncertainty analysis of a single-shot oscilloscope used in calibration of ESD simulators requires knowledge of HF techniques, digital signal processing, and optimization. This challenge is too difficult for calibration laboratories. It motivated the authors to elaborate the subject, show how to cope with an oscilloscope measurement uncertainty, and evaluate it more reasonably. An attempt of such an approach with taking into account the dynamics of the ESD measurement path except the oscilloscope was presented in [6].

Information on the actual frequency response of oscilloscopes' voltage gain is rarely found in the literature. The authors usually conclude that a low-pass second-order filter with damping factor $\zeta \approx 1/\sqrt{2}$ is a satisfactory approximation and compromise for the oscilloscope modeling that can be treated analytically [5].

However, the comparison of such an approximation with actual data presented in [7] and [8] (measured for Tektronix SCD1000) reveals that it is correct only in the passband since the roll off to the stopband is very steep. In these papers, some attempts of taking into account the high-frequency behavior of oscilloscope in the ESD pulse measuring are presented. The starting point of the analysis is the measurement of two frequency-dependent input quantities: 1) reflection $S_{11}(f)$ at the oscilloscope input measured with a vector network analyzer and 2) oscilloscope voltage gain $K_0(f)$ defined as the ratio of the voltage amplitude recorded on the oscilloscope and its true input value. The author [7], [8] uses an analytical formula for the input ESD pulse and applies a so-called sensitivity approach [2] that consists of investigation of how uncertainty of the two measured quantities affect the frequency representation of the recorded voltage.

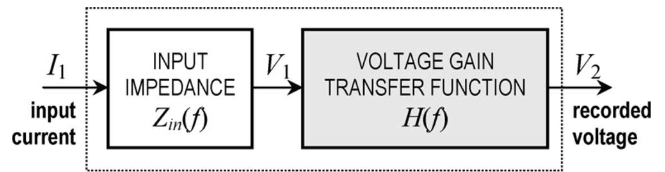

Fig. 4. Dynamic model of oscilloscope: I_1—ESD pulse current and V_2—voltage recorded in oscilloscope memory.

An improvement of this paper over [7] and [8] consists of investigation of how the uncertainty of the measured input quantities is transferred to uncertainty of the pulse metrics (i.e., the rise time and the peak value) in the *time domain*. It is similar to the analysis presented in [5] that deals with dynamic errors of an oscilloscope measurement of the rise time for simpler input signals. To accomplish this aim, we design a more accurate transfer function approximation of the oscilloscope voltage gain that fits the measured frequency response beyond the passband also, and thus, more precisely cover the spectrum of the ESD pulse.

The measured quantities used as inputs are burdened with uncertainty that combines Type A and Type B uncertainties of the calibration laboratory. We use this uncertainty for determining Type B uncertainty of the current pulse parameters. In order to find the pulse time parameters sensitivity, we calculate upper and lower envelopes of the oscilloscope input impedance and voltage gain (which are calculated from measured S_{11} and K_0) in the frequency domain, determine corresponding uncertainties of the pulse metrics, and take the worst case. These are significant improvements in comparison with the approach presented in [7] and [8].

It should be emphasized that analysis presented here is complementary to that in [4]. That is to say, it does not deal with the round-off error and sampling rate uncertainty (see Fig. 3) whose contributions must be added to the overall Type B uncertainty.

II. Dynamic Model of an Oscilloscope

Let us consider an oscilloscope model whose block diagram is shown in Fig. 4. The measured current pulse can be potentially distorted by the oscilloscope input impedance and further by its internal analog and digital circuitry. To carry out the analysis of the dynamic properties of the measurement path, we will be using the following data: 1) reflection coefficient S_{11} at the oscilloscope input measured in the range of 1 MHz–4 GHz (409 frequency points) and 2) magnitude of voltage gain from input voltage V_1 to recorded and displayed voltage V_2 measured in the range of 6 MHz–5 GHz (42 nonuniformly distributed frequency points). The data used in this paper were measured for the LeCroy Wavepro 7300 A 20 GS/s oscilloscope.

The input reflection allows us to calculate the oscilloscope input impedance

$$Z_{\rm in} = Z_g \frac{1 + S_{11}}{1 - S_{11}} \tag{1}$$

Authorized licensed use limited to: IEEE Xplore. Downloaded on November 28, 2008 at 09:03 from IEEE Xplore. Restrictions apply.

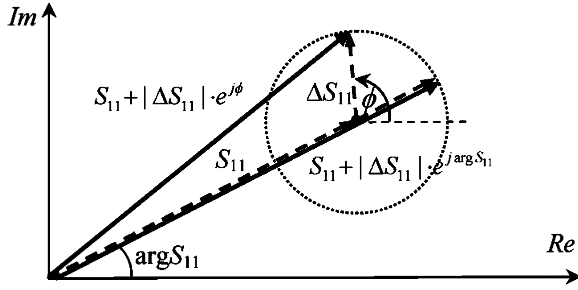

Fig. 5. Two methods of calculating reflection coefficient S_{11} with uncertainty measured as absolute value $|\Delta S_{11}|$. Phase angle ϕ of complex uncertainty $\Delta S_{11} = |\Delta S_{11}|\exp(j\phi)$ is chosen to maximize deviation ΔZ_{in} (2b).

where $Z_g = 50\ \Omega$ is the source impedance of the network analyzer connected to the oscilloscope input port. To extend the analysis to 5 GHz, we extrapolated $Z_{\text{in}}(f)$ above 4 GHz.

Dynamic properties of the path from V_1 to V_2 will be modeled by a transfer function $H(f)$ that not only fits the voltage gain data, but also takes into consideration possible phase shifts as well.

III. Oscilloscope Input Impedance and Its Uncertainty

We take into account the uncertainty of the oscilloscope input impedance Z_{in} related to the measurement uncertainty ΔS_{11} of the oscilloscope input reflection. Since only absolute values of ΔS_{11} are known from the measurements, we consider the following two cases of reconstructing the complex uncertainty of Z_{in}.

1) *Uncertainty of S_{11} maximizes/minimizes the magnitude of input impedance* Z_{in} at each measurement point. By differentiating logarithms of both sides of (1) and assuming that there is no uncertainty on Z_g, we obtain the following relationship for the magnitude of the oscilloscope input impedance uncertainty:

$$|\Delta Z_{\text{in}}| = 2|Z_{\text{in}}|\left|\frac{\Delta S_{11}}{1-S_{11}^2}\right|. \tag{2a}$$

To maximize (minimize) the input impedance magnitude, the complex uncertainty should have the argument of Z_{in} without uncertainty calculated from (1):

$$\Delta Z_{\text{in}} = |\Delta Z_{\text{in}}|e^{j\arg Z_{\text{in}}} = 2Z_{\text{in}}\left|\frac{\Delta S_{11}}{1-S_{11}^2}\right|. \tag{2b}$$

With this approach, the deviations do not change the original phase characteristics of Z_{in}. The given absolute uncertainties of S_{11} are taken into account with some phase angles $\Delta S_{11} = |\Delta S_{11}|\, e^{j\phi}$, which are, in general, different from phase angles of measured S_{11} (see Fig. 5). Adding and subtracting the uncertainty

$$\begin{aligned} Z_{\text{in_max}Z} &= Z_{\text{in}} + \Delta Z_{\text{in}} \\ Z_{\text{in_min}Z} &= Z_{\text{in}} - \Delta Z_{\text{in}} \end{aligned} \tag{3}$$

gives the upper and lower envelopes of magnitude $|Z_{\text{in}}(f)|$, as shown in Fig. 6. The values above 4 GHz were obtained by the nearest neighbor extrapolation.

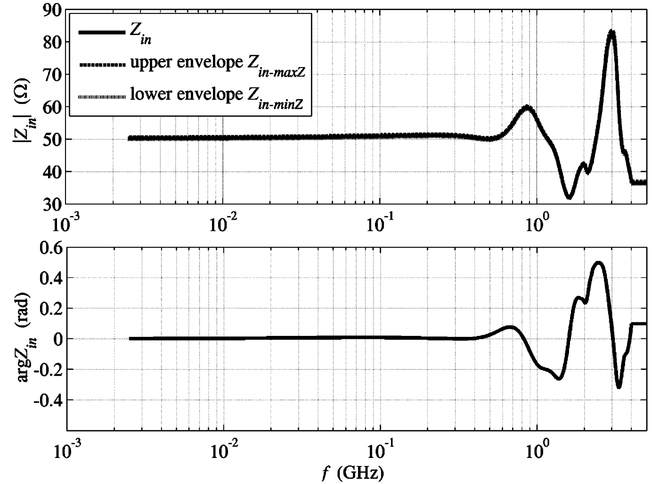

Fig. 6. Magnitude and phase angle of input impedance Z_{in} versus frequency with envelopes (3) obtained by calculating maximum deviations of $|Z_{\text{in}}|$ due to uncertainty of S_{11}.

2) *Uncertainty of S_{11} maximizes/minimizes the magnitude of S_{11} itself.* This is elongation or contraction of vector S_{11} in the complex plane along its original direction so that the phase angle of the reflection coefficient is preserved (see Fig. 5). In this approach, we first determine the envelopes of $S_{11}(f)$, and then, calculate $Z_{\text{in}\Delta}$ with deviations using these envelopes

$$\begin{aligned} Z_{\text{in_max}S} &= Z_{\text{in}\Delta}(S_{11_\text{max}S}),\ S_{11_\text{max}S} = S_{11} + |\Delta S_{11}|e^{j\arg S_{11}} \\ Z_{\text{in_min}S} &= Z_{\text{in}\Delta}(S_{11_\text{min}S}),\ S_{11_\text{min}S} = S_{11} - |\Delta S_{11}|e^{j\arg S_{11}}. \end{aligned} \tag{4}$$

Because the uncertainties are hardly visible in the full scale graph of $Z_{\text{in}}(f)$ in Fig. 6, it is better to look only at its deviations

$$\begin{cases} \Delta Z_{\text{in_max}Z} = \Delta Z_{\text{in}} \\ \Delta Z_{\text{in_min}Z} = -\Delta Z_{\text{in}} \end{cases} \tag{5a}$$

$$\begin{cases} \Delta Z_{\text{in_max}S} = Z_{\text{in_max}S} - Z_{\text{in}} \\ \Delta Z_{\text{in_min}S} = Z_{\text{in_min}S} - Z_{\text{in}}. \end{cases} \tag{5b}$$

The deviations of $Z_{\text{in}}(f)$ calculated using the two methods are presented in Fig. 7(a) and (b).

Note that approach 2) leads to the same uncertainty of the impedance magnitude, but much greater deviations of its phase angle [see Fig. 7(a)]. Therefore, it is the worse case.

IV. Oscilloscope Voltage Gain and Its Uncertainty

A. Approximation of the Voltage Gain by Transfer Functions

The goal is to design a transfer function

$$H(f) = \frac{V_2(f)}{V_1(f)} \tag{6}$$

whose magnitude frequency response is an approximation of the measured oscilloscope voltage gain data

$$K_O(f) = \frac{|V_2(f)|}{|V_1(f)|}. \tag{7}$$

Authorized licensed use limited to: IEEE Xplore. Downloaded on November 28, 2008 at 09:03 from IEEE Xplore. Restrictions apply.

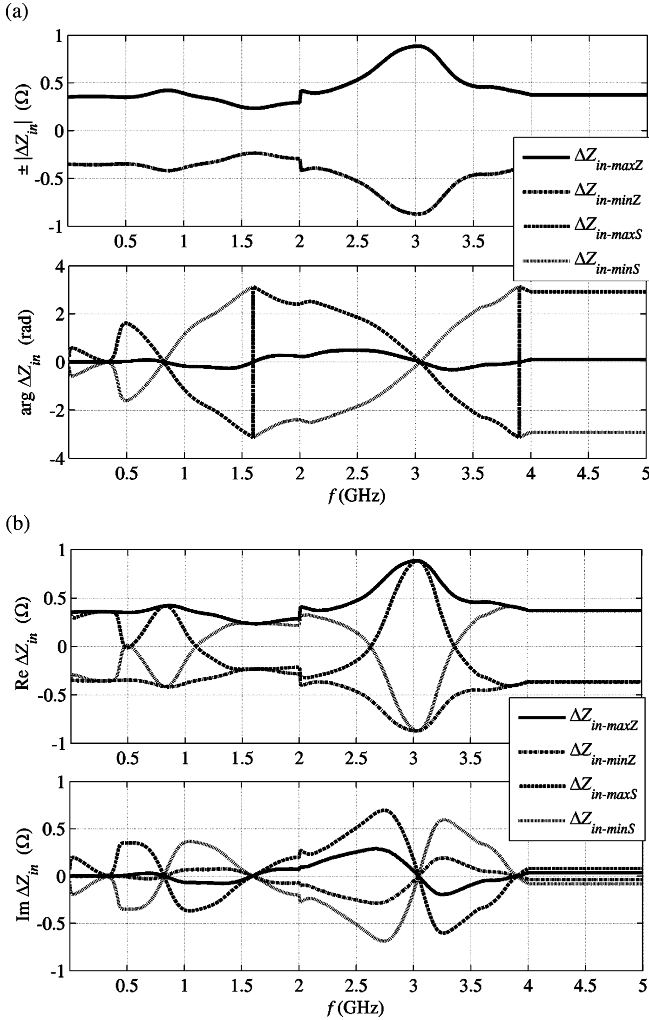

Fig. 7. Deviations of input impedance $Z_{\rm in}$ due to uncertainty of measured parameter S_{11} calculated using the two described methods. (a) Magnitude—phase angle representation (jumps of $\Delta \arg Z_{\rm in}$ occur at $\pm\pi$). (b) Real-–imaginary part representation.

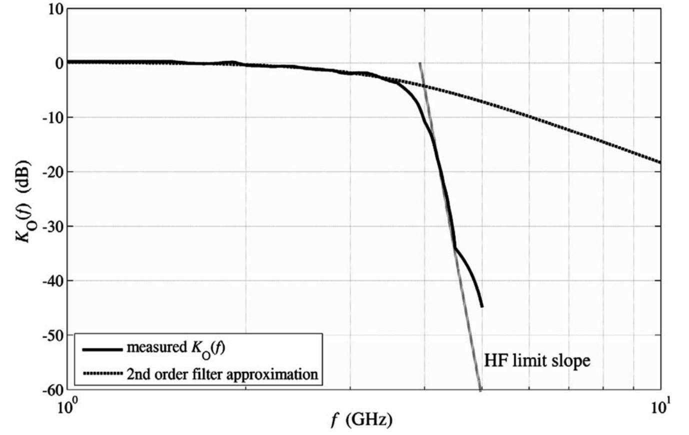

Fig. 8. Asymptotic slope (straight line) of the actual oscilloscope voltage gain magnitude $K_O(f)$ (measured for the LeCroy Wavepro 7300 A oscilloscope) in high frequencies compared with its second-order filter approximation.

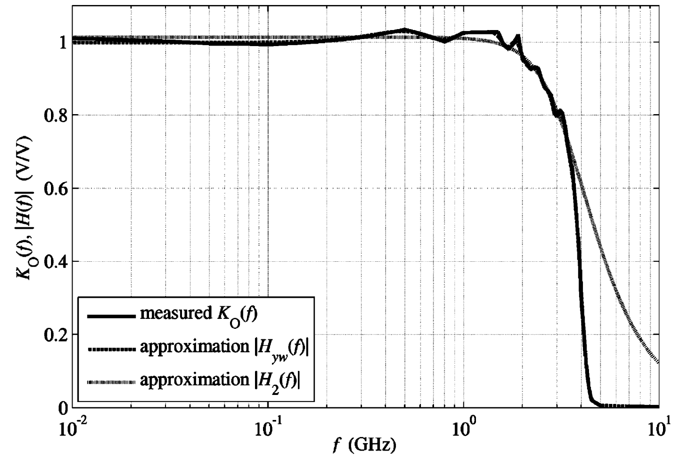

Fig. 9. Approximations of the oscilloscope voltage gain frequency characteristics $K_O(f)$ by a high-order discrete-time filter $H_{\rm yw}(f)$ of order $N = 26$, designed using the Yule–Walker algorithm, and a second-order analog Butterworth filter $H_2(f)$.

It should be emphasized that $H(f)$ is a complex frequency function while $K_O(f)$ represents only the magnitude of the voltage gain response. By using a complex transfer function, we are also able to model the phase shift of the oscilloscope dynamic response. This phase shift is unavailable in our measurements, yet it occurs in reality due to inertia of any electronic circuitry. We limit our interest to the so-called minimal phase transfer functions, because their phase response results directly from the designed magnitude response.

From Fig. 8, we can see that the asymptotic slope of $K_O(f)$ is about -500 dB/decade. This implies that suitable approximation of the steep transition beyond the passband is possible only with a high-order filter since the asymptotic slope is -20 dB/decade for one transfer function pole.

We obtained a very good approximation of the oscilloscope frequency magnitude response by a transfer function of order $N = 26$, employing the function "Yulewalk" from the Matlab's Signal Processing Toolbox [9]. This function designs infinite impulse response (IIR) discrete-time filters

$$H(z) = \frac{b_0 + b_1 z^{-1} + \cdots + b_N z^{-N}}{a_0 + a_1 z^{-1} + \cdots + a_N z^{-N}} = \frac{B(z)}{A(z)} \qquad (8)$$

using the Yule–Walker algorithm [10] to produce a least-squares fit to a specified frequency magnitude response. It returns vectors $B = [b_0, b_1, \ldots, b_N]$ and $A = [a_0, a_1, \ldots, a_N]$, containing $N + 1$ coefficients of the transfer function nominator and denominator. To design a discrete-time filter, it is necessary to specify its sampling frequency f_H. We have chosen $f_H = 20$ GHz, such that the filter Nyquist band (i.e., 10 GHz) exceeds twice the data range. Complex frequency response $H(f)$ of the system described by discrete-time transfer function (8) is obtained by substituting $z = \exp(2\pi jf/f_H)$.

The measured magnitude response $K_0(f)$ and its high-order Yule–Walker approximation $|H_{\rm yw}(f)|$ shown in Fig. 9 nearly overlap. In contrast, the second-order approximation $|H_2(f)|$ designed for comparison (analog Butterworth filter with cutoff frequency $f_n = 3.47$ GHz, damping factor $\zeta = 0.71$, and gain

Authorized licensed use limited to: IEEE Xplore. Downloaded on November 28, 2008 at 09:03 from IEEE Xplore. Restrictions apply.

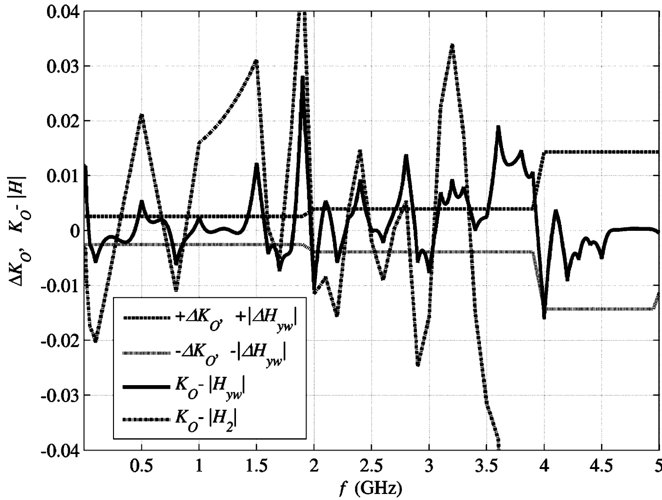

Fig. 10. Differences of magnitudes: uncertainty ΔK_O of the measured voltage gain and magnitude approximation errors $K_O - |H|$ for the designed filters.

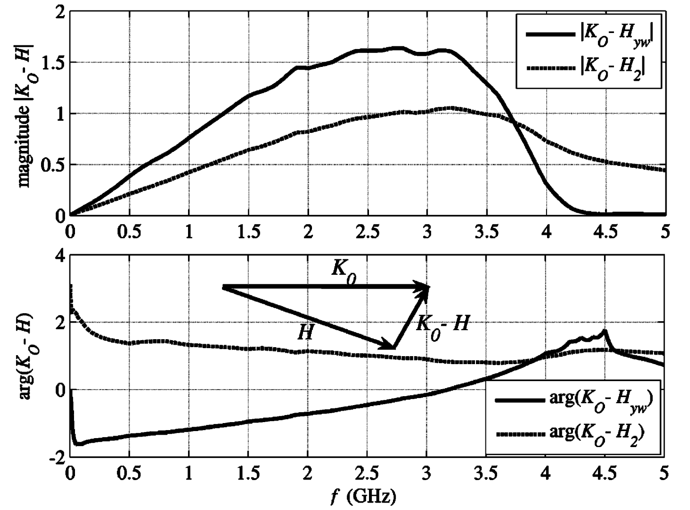

Fig. 11. Magnitude and phase angle of complex differences between the measured voltage gain $K_O(f)$ and its approximations by the designed high-order discrete-time filter $H_{\mathrm{yw}}(f)$ and the second-order analog filter $H_2(f)$.

coefficient $K_2 = 1.01$) cannot be fitted to the measurements above 3 GHz. We should keep in mind that the high-order low-pass filter introduces a significant phase shift that delays high-frequency components of filtered signals.

B. Uncertainty of the Voltage Gain and Its Approximations

In the next step, we take into account the uncertainty of the oscilloscope voltage gain K_O measurements. The data provide only absolute uncertainties ΔK_O, so we are only able to calculate envelopes of the measured characteristics

$$K_{O_\max} = K_O + \Delta K_O$$
$$K_{O_\min} = K_O - \Delta K_O \tag{9}$$

and create envelopes of its transfer function approximation

$$H_{\max} = H + \Delta H, \quad \text{where } \Delta H = \Delta K_O e^{j \arg H}$$
$$H_{\min} = H - \Delta H. \tag{10}$$

The complex deviations of the filter frequency response are calculated along the direction determined by the phase angle of the original complex gain $H(f)$, so they do not change the original phase response.

Fig. 10 shows uncertainty ΔK_O of the measured voltage gain, uncertainty $|\Delta H_{\mathrm{yw}}|$ of the Yule–Walker filter approximation ($|\Delta H_2|$ is omitted due to bigger scale), and magnitude approximation errors $K_O - |H|$ for the two designed filters. The envelopes ΔK_O widen with frequency since the measurement uncertainties of $K_O(f)$ grow with frequency. The envelopes $|\Delta H_{\mathrm{yw}}|$ of the filter approximation are equal to ΔK_O in accordance with definition (10). Although the magnitude envelopes are narrow and the approximation errors are small, the magnitudes of the complex differences $|K_O - H|$ can be quite large due to phase shift of the gain vectors in the complex plane (remember that K_O is real whereas the filters have complex gains). This is shown in Fig. 11. The second-order filter produces smaller magnitude of the difference, because it introduces smaller phase shift than the high-order filter.

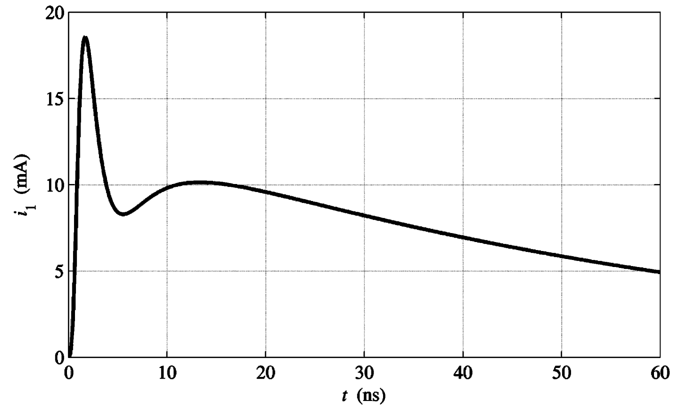

Fig. 12. Theoretical waveform of 5-kV ESD pulse current at the oscilloscope input calculated with the formula proposed in [1] (attenuation × 1000).

V. Uncertainty of ESD Pulse Metrics at the Output of the Oscilloscope Dynamic Model

A. Calculation of the Output ESD Pulse

After specifying the frequency-domain model of an oscilloscope and its uncertainties related to the measurement of the input reflection and the gain voltage, we can consider differences between the ESD input current pulse $i_1(t)$ and the recorded voltage pulse $v_2(t)$ at the model output in terms of the pulse standardized metrics, i.e., the rise time (from 10% to 90% of the peak value) and the peak value. A typical waveform of the model input current calculated with the formula proposed in a standard [3] is shown in Fig. 12. Its rise time is $t_r = 0.85$ ns, and its peak current is $i_{1\mathrm{peak}} = 18.56$ mA. The amplitude is attenuated 1000 times in comparison with the current pulse at the target (see Fig. 1) for convenience due to the range of recorded voltage $v_2(t)$. The overall uncertainty will be calculated for the earlier nominal values.

We transform the current pulse, which was sampled at twice the upper frequency of the data (i.e., 2×5 GHz $= 10$ GHz),

Authorized licensed use limited to: IEEE Xplore. Downloaded on November 28, 2008 at 09:03 from IEEE Xplore. Restrictions apply.

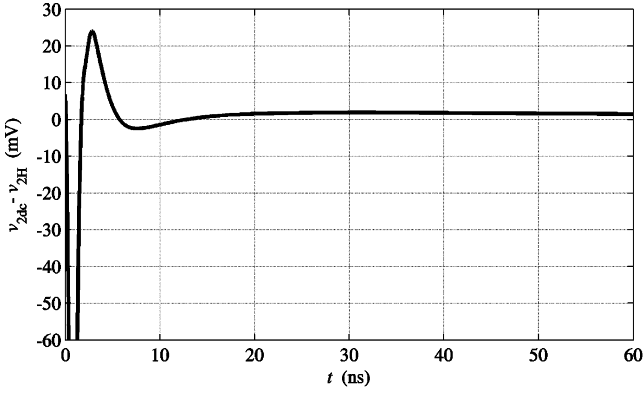

Fig. 13. Difference of output signals produced by the resistance model with $R_{\rm in}$ = constant and the dynamic model with $Z_{\rm in}(f)$ (for which the gain voltage is approximated by $H_{\rm yw}(f)$).

into the frequency domain using the discrete Fourier transform

$$\mathrm{DFT}[i_1(t)] = I_1(f) \tag{11}$$

and calculate the Fourier transforms of the voltages by multiplication in the frequency domain

$$\begin{aligned} V_1(f) &= Z_{\rm in}(f) I_1(f) \\ V_2(f) &= H(f)V_1(f) = H(f)Z_{\rm in}(f)I_1(f) \end{aligned} \tag{12}$$

where $H(f)$ denotes one of the designed voltage gain transfer functions. Finally, we return to the time domain and obtain the output pulse using the inverse transform

$$v_2(t) = \mathrm{ReIDFT}[V_2(f)]. \tag{13}$$

Before the transformations, the measured data are interpolated to the same grid of linearly equidistant frequencies (we used either simple linear interpolation or cubic splines). Then, the Fourier transforms are calculated. Low frequency and dc values are obtained by extrapolating the data toward zero.

The quality of the waveform at the output of the model depends on time window $T_o = M/f_s$ of the signal (M—number of samples and $f_s = 10$ GHz—signal sampling frequency) that must be wide enough to let the pulse fade, and therefore, avoid discontinuity artifacts in DFT and minimize the influence of the transformations on the pulse shape. In the computations, we assumed that $T_o = 400$ ns.

B. Components of the Pulse Metrics Uncertainty

We analyze the influence of the considered dynamic model on $v_2(t)$ with respect to a reference model that assumes a constant input resistance $R_{\rm in}$ of the oscilloscope ($R_{\rm in} = 50.252\ \Omega$ for the LeCroy Wavepro 7300 A oscilloscope) and unit voltage gain transfer function $H(f) = 1$. For this model, it is simply $v_2(t) = v_1(t) = R_{\rm in} i_1(t)$. The dynamic model produces a little distorted output signal. The *difference* of the output signals produced by the two models is shown in Fig. 13. To have a point of reference to the voltage scale in Fig. 13, we should keep in mind that the peak of the output voltage pulse calculated as $v_{2\rm peak} = R_{\rm in} i_{1\rm peak}$ is 933 mV (we use units of the recorded oscilloscope readings). The discrepancy between the waveforms during the first 5–6 ns results from two main reasons: 1) the dynamic model introduces a significant phase shift that distorts steep slopes in the time domain and 2) there are numerical errors (especially near $t = 0$) resulting form the DFT transformation of the pulse to the frequency domain and back.

The following components of the overall Type B relative uncertainty of the pulse metrics $u_{\rm tr}$ (rise time) and $u_{\rm peak}$ (peak value) can be distinguished in our approach (in (14)–(18), below x stands either for tr or peak).

1) Discrepancy between frequency varying complex input impedance $Z_{\rm in}(f)$ versus reference $R_{\rm in}$, voltage gain $H(f) = 1$:

$$u_x = \frac{x(R_{\rm in}) - x(Z_{\rm in})}{x(R_{\rm in})}. \tag{14}$$

2) Uncertainty of $Z_{\rm in}(f)$ due to the uncertainty of S_{11}, calculated either according to (5a) or (5b), voltage gain $H(f) = 1$:

$$u_x = \pm\max\left\{\left|\frac{x(Z_{\rm in}) - x(Z_{\rm in_max}Z)}{x(Z_{\rm in})}\right|, \left|\frac{x(Z_{\rm in}) - x(Z_{\rm in_min}Z)}{x(Z_{\rm in})}\right|\right\} \tag{15a}$$

$$u_x = \pm\max\left\{\left|\frac{x(Z_{\rm in}) - x(Z_{\rm in_max}S)}{x(Z_{\rm in})}\right|, \left|\frac{x(Z_{\rm in}) - x(Z_{\rm in_min}S)}{x(Z_{\rm in})}\right|\right\}. \tag{15b}$$

3) Discrepancy between measured $K_O(f)$ and a complex gain approximation using one of the transfer functions *H(f)*, voltage $V_1 = Z_{\rm in} I_1$:

$$u_x = \frac{x(K_0) - x(H_{yw})}{x(K_0)} \tag{16a}$$

$$u_x = \frac{x(K_0) - x(H_2)}{x(K_0)}. \tag{16b}$$

4) Uncertainty of transfer function approximation *H(f)* due to uncertainty ΔK_O, calculated using envelopes (10), voltage $V_1 = Z_{\rm in} I_1$:

$$u_x = \pm\max\left\{\left|\frac{x(H_{\rm yw}) - x(H_{\rm yw_max})}{x(H_{\rm yw})}\right|, \left|\frac{x(H_{\rm yw}) - x(H_{\rm yw_min})}{x(H_{\rm yw})}\right|\right\} \tag{17a}$$

$$u_x = \pm\max\left\{\left|\frac{x(H_2) - x(H_{2_\rm max})}{x(H_2)}\right|, \left|\frac{x(H_2) - x(H_{2_\rm min})}{x(H_2)}\right|\right\}. \tag{17b}$$

The results are collected in Table I.

We can see that calculating the envelopes of $Z_{\rm in}(f)$ according to (4) (line 2b in Table I), which changes the original frequency phase response, is the worse of the two considered cases and results in significant uncertainty of the rise time as well as in greater uncertainty of the peak value (comparing to values 2a in Table I). In comparison with the second-order analog filter (3b in Table I), the complex gain voltage approximation using the high-order discrete transfer function $H_{\rm yw}(z)$ (3a in Table I) leads to greater uncertainty of the rise time due to a greater phase

Authorized licensed use limited to: IEEE Xplore. Downloaded on November 28, 2008 at 09:03 from IEEE Xplore. Restrictions apply.

TABLE I
COMPONENTS OF THE ESD PULSE METRICS UNCERTAINTY

Uncertainty source	Relative uncertainty (%)	
	u_{tr}	u_{peak}
Input impedance		
1 - real R_{in} vs. complex Z_{in} $H(f)=1$	1.73	-0.62
2a - impedance Z_{in} vs. envelopes Z_{in_minZ}/Z_{in_maxZ}, $H(f)=1$	± 0.00	± 0.70
2b - impedance Z_{in} vs. envelopes Z_{in_minS}/Z_{in_maxS}, $H(f)=1$	± 0.59	± 0.84
Voltage gain		
3a - real K_O vs. complex high order digital approximation H_{yw}	1.18	0.51
3b - real K_O vs. complex second order analog approximation H_2	-0.59	-0.79
4a - filter response H_{yw} vs. envelopes H_{yw_min}/H_{yw_max}	± 0.00	± 0.13
4b - filter response H_2 vs. envelopes H_{2_min}/H_{2_max}	± 0.00	± 0.13

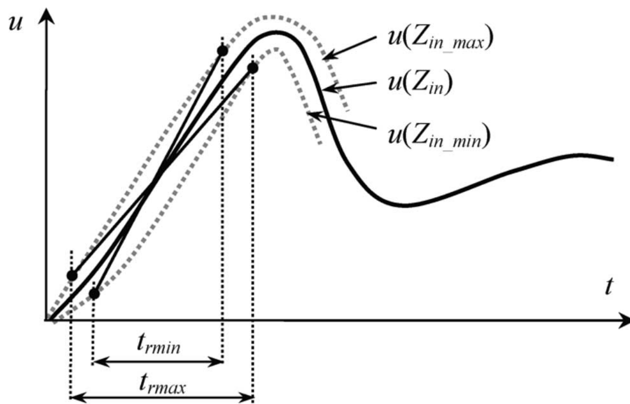

Fig. 14. Method of calculating the rise time uncertainty for the ESD pulses obtained for envelopes of input impedance $Z_{\rm in}$ (the same method was applied for envelopes of transfer function H).

shift but smaller uncertainty of the peak value due to much better approximation of the frequency magnitude response.

The uncertainty of the rise time for components 2 and 4 was calculated by determining the extreme cases between the envelopes, as illustrated in Fig. 14.

The overall expanded uncertainty due to the considered contributions was calculated as the root square sum of the individual components u_{xi}

$$U_x = k\sqrt{\sum_{i=1}^{4} u_{xi}^2} \qquad (18)$$

where $k = 2$ is the coverage factor for the confidence level of 95.5% for the normal distribution.

For the input impedance deviations calculated using (4) and the gain voltage approximated by transfer function $H_{\rm yw}(z)$, we obtain the following expanded uncertainties: $U_{\rm tr} = 4.36\%$ for the rise time and $U_{\rm peak} = 2.32\%$ for the peak value.

VI. CONCLUSION

The contribution of the paper is estimation of uncertainty of the ESD pulse metrics in the time domain (rise time, peak value) due to a frequency-dependent oscilloscope input impedance $Z_{\rm in}$ (calculated from measured input reflection S_{11}) and voltage gain K_O.

The most complicated intermediate task was designing a complex approximation of the oscilloscope voltage gain in order to obtain a good fit to its measured frequency magnitude response K_O, not only in the passband, but also over the whole frequency range, and to take into account the phase shift that was not available from the measurements. We achieved this by designing a high-order discrete-time transfer function $H(z)$ using the Yule–Walker method.

The measurement uncertainties of the oscilloscope input reflection and the voltage gain were used for building upper and lower envelopes of the oscilloscope input impedance and voltage gain approximation, respectively (i.e., maximize or minimize the enveloped quantities). The envelopes enabled us to calculate another uncertainty contribution, which is the sensitivity of the ESD pulse metrics to the measured quantities. The deviations of the metrics were calculated twice for the upper and lower envelopes, and the worse case was taken as the uncertainty estimation. Finally, the overall expanded uncertainty of the pulse metrics was determined on the basis of the proposed model as the root square sum of the four contributions.

Almost all low-frequency uncertainties of the oscilloscope that can be usually found in the manuals (vertical accuracy, vertical linearity, offset accuracy, horizontal accuracy) are incorporated in the approach presented here. Therefore, they do not have to be root square summed with other uncertainty contributions. Solely, the round-off error and sampling rate errors must be added to the vertical and horizontal uncertainties, respectively. The sampling rate uncertainty of the rise time that we calculated for 20 GS/s is 20.4 ps with respect to 850 ps slope (it yields 4.8%, expanded with coverage factor $k = 2$).

In our opinion, the features listed earlier make the uncertainty estimation approach presented in the paper more precise than those published up till now.

ACKNOWLEDGMENT

The authors would like to thank Prof. D. Pommerenke, Missouri University of Science and Technology, for his fruitful consulting.

REFERENCES

[1] *Electromagnetic Compatibility (EMC)—Part 4–2: Testing and Measuring Techniques—Electrostatic Discharge Immunity Test*, IEC Standard 61000–4-2, May 1999.
[2] *Expression of the Uncertainty of Measurement in Calibration*, European Co-operation for Accreditation, Document EA-4/02, Dec. 1999.
[3] *Electromagnetic Compatibility (EMC)—Part 4–2: Testing and Measuring Techniques—Electrostatic Discharge Immunity Test*, IEC Standard 77B/563/CDV 61000–4-2, Dec. 2007.
[4] T. Kang, Y. Chung, S. Won, and H. Kim, "On the uncertainty in the current waveform measurement of an ESD generator," *IEEE Trans. Electromagn. Compat.*, vol. 42, no. 4, pp. 405–413, Nov. 2000.

Authorized licensed use limited to: IEEE Xplore. Downloaded on November 28, 2008 at 09:03 from IEEE Xplore. Restrictions apply.

[5] Ch. Mittenmayer and A. Steininger, “On the determination of dynamic errors for rise time measurement with an oscilloscope,” *IEEE Trans. Instrum. Meas.*, vol. 48, no. 6, pp. 1103–1107, Dec. 1999.
[6] J. Baran, T. Drozdz, and J. Sroka, “Transfer impedance model of measurement path for ESD simulator calibration,” in *Proc. 18th Int. Wroclaw Symp. Exhib. EMC*, Wroclaw, Poland, Jun. 2006, pp. 151–156.
[7] J. Sroka, “Oscilloscope influence on the calibration uncertainty of the peak current of ESD simulators,” presented at the 17th Int. Zurich Symp. EMC, Zurich, Switzerland, Feb. 2003.
[8] J. Sroka, “Oscilloscope influence on the calibration uncertainty of the pulse rise time of ESD simulators,” in *Proc. 2003 IEEE Int. Symp. EMC*, Istanbul, Turkey, May 2003, pp. 378–381.
[9] *Signal Processing Toolbox User’s Guide. Ver.4,* The Mathworks, Inc., Natick, MA, 1998.
[10] J. G. Proakis and D. G. Manloakis, *Digital Signal Processing: Principles, Algorithms and Applications*. Englewood Cliffs, NJ: Prentice-Hall, 1996.

Janusz Baran was born in Czestochowa, Poland, in 1961. He received the M.Sc. degree in electrical engineering from Czestochowa Technical University, Czestochowa, Poland, in 1985, and the Ph.D. degree in electrical engineering from Lublin Technical University, Lublin, Poland, in 1990.

Since 1986, he has been with the Institute of Electronics and Control Systems, Czestochowa Technical University. His current research interests include signal processing, digital control, and adaptive systems.

Jan Sroka (M’01–SM’05) was born in Szczerców, Poland, in 1952. He received the M.Sc., Ph.D., and D.Sc. degrees in electrical engineering from the Warsaw University of Technology, Warsaw, Poland, in 1974, 1982, and 1991, respectively.

From 1994 till 2005, he had been with SCHAFFNER EMC AG, Switzerland, in the Research and Technology Department, Component Development Department, and Test Systems Department. In 2006, he joined the EMC-Testcenter Zurich AG, Zurich, Switzerland. His current research interests include investigation of the electrostatic discharge phenomenon as well as establishment of uncertainty budget in EMC calibration and testing.

Authorized licensed use limited to: IEEE Xplore. Downloaded on November 28, 2008 at 09:03 from IEEE Xplore. Restrictions apply.